Synergistic Coupling of Molybdenum Carbide Nano-sphere with Pt Nanoparticles for Enhanced Ammonia Electro-oxidation Activity in Alkaline Media

Maryam Bayati,[Δ*] Xiaoteng Liu, [‡] Patricia Abellan,[#] Dan Pocock, [†]Michael Dixon, [§] Keith Scott[◊]

Δ* Department of Engineering and Mathematics, Sheffield Hallam University, S11WB, UK, [‡] Department of Mechanical & Construction Engineering, Northumbria University, NE1 8ST, UK, # SuperSTEM Laboratory, SciTech Daresbury Campus, Daresbury, WA4 4FS, UK,† Sellafield Ltd, Cumbria, CA20 1PG, UK, § Hitachi High-Technologies Europe, Daresbury, WA4 4AB, UK, ◊ Department of Engineering, Newcastle University, Newcastle, NE1 7RU, UK

KEYWORDS Ammonia Electro-oxidation, Fuel cell, molybdenum carbide, platinum nanoparticles, synergistic effect

ABSTRACT Ammonia will play a pivotal role in the future of zero carbon emitted sustainable fuel. The development of inexpensive efficient catalysts for ammonia electro-oxidation (AEO) is essential to its success. This study provides evidence that nanoparticles of earth-abundant elements, e.g. MoC, encapsulated in a doped-graphene shell (DG-MoC) are promising co-

catalysts of Pt for AEO which significantly improves the catalyst cost and activity in comparison to the state of art platinum. DG-MoC, DG-MoC-supported Pt (Pt/DG-MoC) and nitrogen-doped-graphene (NG) catalysts were synthesized and characterized by Brunauer–Emmett–Teller (BET) surface area analysis, electrochemical techniques, X-ray photoelectron spectroscopy (XPS), X-ray diffraction (XRD), Scanning Electron microscopy (SEM) combined with Energy-dispersive X-ray (EDX), Scanning transmission electron microscopy (STEM) and electron energy loss (EEL) spectroscopy. The XRD analysis of DG-MoC disclosed the presence of α-MoC_{1-x} Microscopy techniques demonstrate a close vicinity of Pt and MoC nanoparticles in Pt/DG-MoC. We report, for the first time, that Pt/DG-MoC particles reveal a large synergistic effect for AEO activity whilst DG-MoC and NG showed no activity. Pt/DG-MoC gave a higher current density, lower half- and peak- potentials (28 mV and 14 mV respectively) and greater resilience to ammonia poisoning than Pt/C as shown in fall in the peak current density in the second voltammogram, i.e, approximately 3.6%, compare to 20.7% for Pt/C. The XPS spectrum of the catalysts explained the source of this synergistic effect.

1. INTRODUCTION

Ammonia electro-oxidation has received considerable attention for its applications in ammonia low-temperature fuel cells (AFCs)[1-4], production of high-purity hydrogen,[5-6] electrochemical removal of ammonia in wastewater[7-8] and fabrication of electrochemical sensors[9].

Ammonia, in comparison to methanol, is a carbon-free energy carrier, with higher hydrogen storage capacity (17.7 wt%), oxidation charge, energy density(3000Wh kg^{-1}) and low production cost (1.2 $/kWh and 3.8 $/kWh for ammonia and methanol, respectively). Ammonia is the second most commonly produced chemical in the world and a large infrastructure for its

synthesis, transportation, and distribution exist. Moreover, ammonia decomposition generates hydrogen, another energy vector, which theoretically should cost less than the one currently produced from water electrolysis[10-11]. These advantages make ammonia a promising fuel for low/medium-temperature AFC to combat the global challenges of carbon emission and fossil fuel depletion. To date, the most effective catalyst for AEO has been platinum and its alloys with other noble metals such as Ir. The high cost and scarcity of these catalysts present major technical challenges which limit the commercialization of AFC. Therefore, significant efforts are devoted to develop catalysts with low Pt loading. This has been achieved by a) alloying it with less expensive metals, b) increasing Pt mass activity by developing catalysts with higher surface area and more active sites, c) exploring supports with great synergistic impact on the catalytic activity of Pt. The latter approach is the focus of this work.

It is well-known that high-surface-area metal carbides and nitrides, particularly of the group VI transition metals, possess catalytic properties comparable to those of noble metal catalysts. These properties, along with their good chemical resistivity and electric conductivity, make them promising catalysts. These compounds have been extensively investigated for a number of reactions as catalysts[12-14] or catalyst supports[15-16] including hydrogenation[17], dehydrogenation[18], methane to syn-gas conversion[19], hydrogen evolution[20-22], ammonia decomposition[23-24] and synthesis[25-26]. It has been found that for the latter two reactions, the nitrogen-metal interaction plays a pivotal role in the catalytic activity[23-28] and in particular, molybdenum showed high activity. Density function theory (DFT) calculations of the catalytic efficiency of the transition metals for the synthesis[29] and decomposition[30] of ammonia show that the efficiency is associated with the chemisorptions energy of nitrogen. Thus, molybdenum carbides are considered as excellent catalysts for both reactions at elevated temperatures.

At low temperature, molybdenum carbides do not show great activity. However, as a support, α-MoC, β-Mo_2C, γ-MoC, and η-MoC, reveal a synergistic impact in some reactions at ambient temperatures and thus have been employed as promoters of noble metal electro-catalysts. It has been reported that their composites with Pt or Pd demonstrate comparable or even greater activity toward the oxygen reduction reaction (ORR)[31-33], methanol oxidation[31] and water gas shift reaction[34] with their ability to provide hydroxyl groups by dissociating O–H bonds (e.g. on MoC next to Pt) and reacting as a co-catalyst.

Herein, for the first time to our knowledge, we demonstrate that high surface area α-MoC_{1-x} promotes Pt and the resulted Pt/DG-MoC composite is a promising high efficient catalyst for AEO at ambient temperature.

In order to synthesize the catalyst, Phosphomolybdate (PMo_{12}) was used as a Mo precursor. However, due to the high temperature required for the synthesis of molybdenum carbide, sintering and aggregation of the particles, the specific surface area and therefore the number of active sites[35] are reduced. To overcome this drawback, a highly porous, conductive and chemically stable support of GO can be employed[36]. It is demonstrated that the presence of electrostatically adsorbed ionic phosphomolybdate between negatively charged GO nano-sheet prevents π-stacking agglomeration of graphene as well, which leads to a porous and well-dispersed nano-structured catalyst[20,21,37,38].The preparation method is described in Scheme 1.

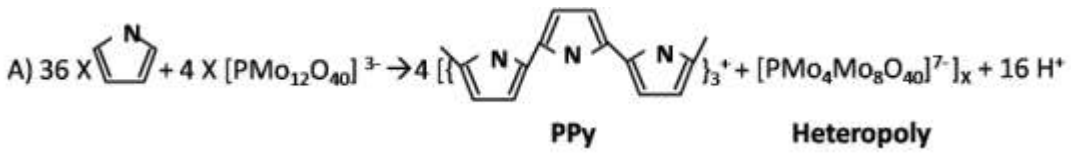

Scheme 1. Two step formation of PMo12−PPy/RGO nano-composite. A) Production of heteropoly and polypyrrole. B) Reduction of GO by heteropoly.

The phosphomolybdate is further reduced with pyrrole (Py) to produce heteropoly blue, which is further used for the reduction of graphene oxide accompanied by formation of polypyrrole (PPy). Pyrolysis of the composite produces molybdenum carbide via carbothermal reduction of molybdate and generates gaseous carbon mono- and di-oxide, leading to the formation of the final porous structure[39]. The porous morphology increases the surface area and the reactants mass transfer. Concomitantly, carburizing of PPy leaves few protecting graphene layers around molybdenum carbide nanoparticles and prevents their agglomeration. Herein, our investigation on this high surface area HSG-Mo as a catalyst and support for Pt nanoparticles revealed a large synergistic effect, while DG-MoC showed no significant activity toward AEO at ambient temperature.

2. EXPERIMENTAL SECTION

2.1. Materials and Instrumentation

The electrochemical measurements were carried out with an Autolab potentiostat, PGSTAT302N, Methrohm Autolab B. V. A platinum coil was used as the counter electrode; the potentials were measured and reported with respect to a silver/silver chloride reference electrode (3 M NaCl) (for ease of comparison in 0.2 M NaOH, $E_{RHE} = E_{Ag/AgCl,3MNaCl} + 1.09$ V). All measurements were performed at a temperature of 25◦C. The electrochemical experiments for AEO were conducted in N_2 saturated 0.2 M NaOH + 0.1M NH_3 solution. Solutions were prepared with de-ionized water and purged with nitrogen (BOC, 99.998%) for 20 min before each experiment, and a blanket of it was kept during the experiments. A three-electrode cell was

employed for the electrochemical measurements on a GC disk electrode from ALS Co., Japan. The electrode was cleaned initially by polishing with alumina powder (1.0, 0.3and 0.05 mm diameter, Buehler GmbH, Germany) on a cotton wool polishing cloth (Buehler, GmbH, Germany) and rinsed with de-ionized water. The cleaning procedure was followed by sonication in water for 20 min and repeated before each electrochemical measurement. The electrode was prepared by mixing 10 mg of catalyst, 2.25 ml of de-ionized water/ethanol and 0.25 ml of 5% ionomer solution in an ultrasonic bath and placing the required amounts of the catalyst suspension on the mirror-polished glassy carbon disk at a loading of 0.3 mg cm^{-2} and finally left in air to dry. A 10% Pt–C catalyst was also used as a reference sample.

XPS was performed using a K-Alpha-spectrometer (NEXUS, Newcastle University, UK) employing an AlKα X-ray source. The spectra were collected with a band-pass energy of 20 eV, which is typical for high-resolution conditions. The binding energies (BEs) were referenced to and calibrated against C 1s (284.5 eV). The results were analyzed based on National Institute of Standards and Technology (NIST) database.

High resolution bright field (BF), high angle annular dark field (HAADF) STEM imaging and EELS were performed using a Cs-corrected Nion UltraSTEM 100 operating at 100kV and equipped with a Gatan Enfina spectrometer (Gatan Inc., Pleaseanton, CA). The microscope is equipped with a cold field emission electron emitter, providing a native beam energy width of 0.3 eV (full-width at half-maximum). The probe size was ~0.1 nm, probe convergence semi-angle was 32 mrad, the Electron energy-loss spectroscopy (EELS) collection semi-angle was 37mrad and the HAADF collection semi-angular range was 80-185 mrad. Prior to STEM imaging, the samples were baked for 12 hours in vacuum at 130◦C to reduce hydrocarbon contamination. In order to improve signal-to-noise, vertical binning (100x) was used for all core-

loss measurements. To generate the chemical maps revealing the relative element concentrations, EELS data was processed using the Gatan Digital Micrograph (DM) software suite: a standard (power law) background was subtracted from all spectra prior to signal integration over suitable energy windows above the elements' edge onsets. Fourier transform (FT) analysis of high resolution images of individual nanoparticles was performed using Gatan DM software. To ensure accuracy, a re-calibration of the images scale was done using images from a standard Au nanoparticles sample recorded before carrying out the sample measurements.

SEM imaging was carried out using a Regulus 8230 cold field emission CFE-SEM and Hitachi SU9000 equipped with a high-efficiency Bruker Flat Quad EDX detector (Hitachi High-Technologies Europe). A dilute suspension of the catalysts in ethanol was drop cast on lacy carbon grid, dried and used for imaging.

XRD pattern was recorded on a PAN analytical X'Pert Pro MPD diffractometer using Cu Ka radiation. BET measurement and analysis ran employing a Thermo Scientific Surfer instrument using N_2 gas. Phosphomolybdic acid hydrate (Acros Organics, 80%), sodium borohydride (BDH, 98%), chloroplatinic acid (Sigma-Aldrich, >99.9%), 4% wt ionomer (Acta), oxidized graphene oxide powder (Aldrich, 15-20 sheets 4-10% edge), platinum on carbon black (Alfa Aesar, 10%), pyrrole (Sigma-Aldrich, >98%), absolute ethanol (Fisher Scientific), sulfuric acid (Sigma-Aldrich, 99.99%), ammonia (Aldrich) and sodium hydroxide (Sigma-Aldrich, 99%) were used as received.

2.2. Synthesis of DG-MoC

GO nano-sheets were dispersed in de-ionized water by ultrasonication to make a 1000 ppm suspension. 12.5 ml of the suspension and 150 ml of 2mM PMo_{12} solution were mixed, under

strong ultrasonication. A solution of 230 µl of Pyrrole in 15ml deionized water was then gradually dropped into this suspension. The mixture colour gradually changed from yellowish-brown to dark blue and after about 7 min a black precipitate began to appear. Finally, the flask was transferred to an oil bath and the reaction was continued for 30 h at 50 ◦C under vigorous magnetic stirring. Subsequently, the black precipitate was separated by centrifugation, washed with deionized water and anhydrous ethanol several times and dried in vacuum at 50 ◦C. To prepare the DG-MoC nano-composite, 2 g of the black precipitate was carbonized in a controlled-atmosphere furnace under continuous flow of pure N_2 at 900 ◦ C for 2 h with a heating ramp of 5 ◦Cmin^{-1}. The carbonized sample was acid etched in 0.5 M H_2SO_4 for 24 h with continuous agitation at 80 ◦C to remove side-products. The sample was then washed with deionized water until reaching a neutral pH.

2.3. Synthesis of Nitrogen Doped Graphene

A dispersion of 1000 ppm of GO nano-sheets in deionized water was made by ultrasonication for half an hour at room temperature. While stirring vigorously, a solution of 230 µl of Pyrrole in 15 ml deionized water was added drop-wise into 12.5 ml of the suspension. Subsequently, 150 ml solution of $FeCl_3$ ($FeCl_3$/ pyrrole with a mole ratio of 2) was slowly added under stirring to the suspension. The colour of the mixture gradually changed from yellowish-brown to blue and a black precipitate began to appear after a few minutes. The polymerization reaction was continued under stirring for 24 h. The resulting black precipitate was centrifuged and washed with ethanol and deionized water in sequence several times. Finally the precipitate was dried under vacuum at 50 ℃ overnight and, in a similar procedure to the preparation of DG-MoC, carbonized in a controlled-atmosphere furnace under continuous flow of pure N_2 at 900 ◦C for 2 h with a heating ramp of 5 ◦Cmin^{-1}. The carbonized sample was acid etched in 0.5 M H_2SO_4 for 24 h with

continuous stirring at 80 ◦ C to remove the iron compounds. The sample was then washed with de-ionized water until reaching a neutral pH.

2.4. Synthesis of Pt/DG-MoC and Pt/NG

1 g of DG-MoC was dispersed in 200 ml de-ionized water and sonicated for 15 min. An adequate amount of H_2PtCl_6 was added to prepare a DG-MoC solution containing10% Wt% Pt and the solution stirred for 10 min. 50 ml $NaBH_4$ with a 10 fold molar ratio of Pt was added drop-wise while the solution was being stirred vigorously. Stirring continued for 20 more minutes and finally the precipitate was separated using a centrifuge and washed with deionized water to reach a neutral pH. Pt/DG-MoC was dried at 50 ◦C. To synthesis Pt/NG, a similar procedure was followed except NG instead of DG-MoC was used.

3. RESULTS AND DISCUSSION

3.1. BET Measurements and XRD Characterization

The high surface area of DG-MoC and NG was measured with BET analysis method as one of the main specifications of a suitable substrate. The measured surface areas of DG-MoC and NG were 150 and 560 m^2g^{-1}respectively. This indicates that as previously reported for porous molybdenum carbides,[38] these are very porous supports. The crystal structure of NG, DG-MoC and Pt/DG-MoC was investigated by XRD (Fig. 1). The peak broadening of DG-MoC and Pt/DG-MoC is explained by the small size of nanoparticles, as can be seen from their electron microscopy images (Fig. 2 and 3). The XRD pattern of DG-MoC displays characteristic diffraction peaks at 2Θ of 36.7◦, 42.3◦, 61.3◦ and 73.9◦. Although slightly shifted in absolute terms, these are very close to the (111), (200), (220), (311) and (222) reflections of the face-centered cubic (fcc) crystalline structure of α-MoC_{1-x}[31, 25] (located at 36.4◦, 42.3◦, 61.3◦ and 73.5◦). Importantly, these diffraction peaks are not comparable to patterns of other molybdenum

carbide compounds such as γ-MoC, η-MoC and β-Mo_2C[40-42]. A similar small shift from α-MoC_{1-x} pattern was observed in molybdenum carbide compounds doped with a small quantity of nitrogen at elevated temperature[40]. It was found by Qiua *et al.* that a further increase in the carburizing temperature in the presence of nitrogenous compounds leads to a complete substitution of nitrogen and the formation of a molybdenum nitride phase. Therefore, the small observed shift can be associated with slight nitrogen doping of molybdenum carbide from pyrrole[40]. The main characteristic XRD peaks in Pt/DG-MoC were observed at 39.79◦, 46.21◦, 67.77◦, 81.28◦ and 85.96◦, correspond to (111), (200), (220), (311), and (222) planes of fcc platinum. This confirms the formation of Pt nanoparticles (a = b = c = 3.8920Å) (JCPDS number, 05-0681)[43]. A small shoulder at 2Θ of approximately 36.5◦ arises from the presence of DG-MoC substrate. XRD of NG shows two significant diffraction peaks at 2Θ=26.5◦ and an overlapped peak area between 2Θ=43◦ and 44.58◦, which are attributed to the (002) reflection of graphitic carbon and the overlapped reflections of the C(101) and C(100) planes of a typical turbostratic carbon structure, respectively[44-45]. This suggests that the GO was efficiently reduced during the hydrothermal process.

3.2. Electron Microscopy Characterization

The morphology and microstructure of DG-MoC were investigated by SEM and STEM (Fig. 2 and Supporting Information Fig. S1). SEM images (Figure 2A) reveal that the HSG support consists of nano-spheres of 70-100 nm diameters. Dark field (DF) SEM images showed smaller nanoparticles dispersed throughout the nano-spheres (Fig. 2B). EDX mapping revealed that the nanoparticles were mainly composed of Mo (Fig. 2C) and carbon (Fig. S1 in supporting information). The high resolution image shows that these nanoparticles have a diameter of approximately 2-10 nm and are surrounded by porous layers of graphene (Fig.1D), which

explains the high surface area of the catalyst and facilitates electron conductivity within the catalysts. EELS is a valuable technique for detecting carbides and nitrides of transition metals and for resolving their spatial distribution at the nanoscale. In our case, however, the Mo, M4,5-edge (at *ca.* 227 eV) and M2-edge and M3-edge (peaks at ca. 392 and 410eV respectively) overlap with the N K-edge (at ca. 401 eV) and C K-edge (at ca. 284 eV) which can make the data interpretation challenging. To demonstrate the presence of Mo, the EELS spectra acquisition in the area with (blue line) and without molybdenum (red line) were carried out (Fig. 2E). The presence of Mo was confirmed by the presence of an intensity shoulder at the foot of the carbon K edge (labelled Mo M4,5) which is only observed in the Mo-contained area. The fine structure of the CK edge in this spectra is consistent with a graphitic carbon structure, with characteristically sharp π* and σ* peaks. A High-angle annular dark-field (HAADF) image of a nanoparticle near the surface and its corresponding Fourier Transform (FFT) (inset) are presented in Figure 2F. The observed Fourier spots are indexed as being consistent with a molybdenum carbide crystalline structure viewed along the {011} one axis. The nanoparticles are partly faceted (dashed lines) on low index planes, {111} and {200} with the corresponding measured d-spacings of 2.45 Å and2.13 Å respectively, support the XRD results that indicate an α-MoC_{1-x} structure.

SEM images of platinized molybdenum carbide nanoparticles, Pt/DG-MoC, revealed a high dispersion of Pt nanoparticles on molybdenum carbide nanomaterials (Fig. 3A). This can be explained by the interaction between the platinum salt and the porous surface of the molybdenum carbide on graphene,[46-47] that results in the nucleation of individual platinum metal clusters. Theoretical calculations indicate that the binding energy of Pt to molybdenum carbide is 0.9 eV lower than the cohesive energy of Pt[47]. EDX mapping of Pt/DG-MoC catalyst reveals the close

contact between the molybdenum carbide and the Pt nanoparticles (Fig. 3B, 3C and 3D). EEL spectra were recorded in areas containing only the doped graphitic matrix, free from nanoparticles (Fig. 3E), with molybdenum carbide (Figs. 3F and 3G) and from the outer part of platinum nanoparticles (Fig. 3H). These spectra reveal the presence of both molybdenum carbide and Pt nanoparticles (see details of the averaged areas and spectra collection in Fig. S2).

3.3. Chemical Composition Investigations

Table 1. Binding Energies in DG-MoC

Elements	Peak Binding Energies/eV	Oxidation States/ species*
Mo	228.3, 229.2, 231.2, 232.6	Mo^{2+}, Mo^{3+}, Mo^{5+}, Mo^{6+}
N	396.8, 398.3, 399.5, 400.8	Mo-N, pyridinic, pyrrolic and quaternary nitrogen
P	130.1, 132.8, 133.7	P 2p3/2 of Mo-P, P-C and P-O

* Oxidation states/functionalities referring to the binding energies of the previous column in the same order.

Details of the catalysts chemical composition were investigated by XPS.The survey spectra of the catalysts (Fig. 4A) show characteristic peaks of O 1s, C 1s, and N 1s, P 2p, Mo 3d and Mo 3p which suggests the incorporation of N and P atoms as well as Mo in the DG-MoC structure (Fig. 4A-I), and Pt appears only in Pt/DG-MoC (Fig. 4A-II). Deconvolution of the Mo 3d spectrum in DG-MoC revealed eight peaks associated with Mo^{2+}(228.3 eV), Mo^{3+}(229.2 eV), Mo^{5+} (231.2 eV) and Mo^{6+} (232.6 eV) oxidation states (Fig.4B-II) with each species splitting into 3d5/2 and 3d3/2 peaks (spin–orbital splitting of ~3.15±0.2 eV), in accordance with the literature [38-48]. The analysis was carried out based on the area ratio of [Mo^{n+} 3d5/2] / [Mo^{n+} 3d3/2] = 3/2 and at the

above mentioned value for the spin-orbit splitting. Mo^{2+}, Mo^{3+}, Mo^{5+} and Mo^{6+} oxidation states can be linked to the presence of the carbide, phosphide or nitride and oxide species, respectively (Table 1). This, provide further evidence of the successful synthesis of molybdenum carbide as the catalyst. Figure 4C displays the four deconvoluted peaks of N1s at binding energies of 396.8, 398.3, 399.5 and 400.8eV, which are assigned to Mo-N, pyridinic, pyrrolic and quaternary nitrogen functionalities in DG-MoC [49-50] (Table 1).The analysis of the signal in the phosphorous region of the spectrum was carried out based on the area ratio of [P^n 2p3/2] / [P^n 2p1/2] = 2/1 and a value of ~0.87±0.2 eV as the spin-orbit splitting. Hereafter these are referred to as the P 2p1/2 and P 2p3/2 signals for simplicity. The peak at 394.6 eV is associated with Mo 3P [51]. The doublet at 129.2 eV and 130.1 eV in the P 2p region (Fig. 4D) is associated with Mo-P bonding (Table 1) which strongly suggests molybdenum carbide is being slightly doped with phosphorous [52]. The signals at binding energies of 132.8 and 133.7 eV are attributed to P 2p3/2 of P-C and P-O respectively [38,53,54] and reveals a partial doping of the graphene matrix and some oxidation of the catalyst. Therefore, the XPS analysis further confirms nitrogen and phosphorous doping of the molybdenum carbide as well as in the carbon matrix. The XPS spectrum in the molybdenum region of platinized DG-MoC catalyst shows a shift of approximately 0.49 eV to lower bonding energies (Fig. 3B-I) as compared with those taken from the DG-MoC catalyst, thus indicating an interaction between the molybdenum and platinum nanoparticles. A similar shift in the XPS spectrum as a consequence of electronic interaction between metal-support has been previously reported [55,56] which consequently results in modified chemical properties. Our results on partial charge transfer from Pt to molybdenum are consistent with Li`s group observation of Pt/Mo_2C catalyst which indicates an increase in binding energies of Pt as a nano-layer on Mo_2C substrate [57-58]. These findings are in line with the electron afinity of the metals and substrates. Young *et al*.

showed that Mo in molybdenum carbide is positively charged due to charge transfer from Mo to C atom [59] which promotes charging platinum nanoparticles. This ligand effect which results from orbital interaction between a deposited metal and its support, induces an electronic charge transfer at the interface, modifies the chemical properties of the catalysts as we observed at this work.

3.4. Electrochemical Activity Investigations

The electrocatalytic performance of the three as-prepared NG, DG-MoC and Pt/DG-MoC catalysts was evaluated for ammonia oxidation in an alkaline solution in the absence and presence of ammonia (0.2 M NaOH and 0.2 M NaOH + 0.1M NH_3 solutions). The results are presented in Figure 5 along with the cyclic voltammogram of 10 wt % Pt/C for comparison. The polarization curves of NG and DG-MoC catalysts are shown at higher magnification in the inset. As can be seen, NG and DG-MoC do not show any fine feature of hydrogen adsorption and desorption reactions, nor any ammonia oxidation peak. This indicates they are catalytically inactive for these reactions. The fine features in hydrogen adsorption and desorption region of platinum cyclic voltammogarms changed by employing DG-MoC as a substrate in Pt/DG-MoC catalyst. This indicates an interaction between the substrate and platinum nanoparticles. It is noteworthy that such an interaction did not observe in presence of NG (Figure S3). Figure 5A shows two consecutive oxidation cycles in ammonia solution for Pt/ DG-MoC and Pt/C. The platinized molybdenum carbide samples exhibit a larger activity; Pt/DG-MoC generates approximately 23% higher current in the first cycle at the peak potential in compared to Pt/C. A similar effect has been observed previously with some rare earth metal oxides as substrates [60]. Peak potential and half peak potential (E1/2) of Pt/DG-MoC are also 28 mV and 14 mV respectively lower than peak potential and E1/2 of Pt/C catalyst (Figure 5B). To check the

catalytic impact of NG on Pt for AEO, a control experiment with NG supported Pt was carried out under the similar condition which the results did not revealed any synergistic effect (Fig S3).

Therefore the increase in current of bifunctional Pt/DG-MoC catalyst can be explained by the presence of MoC_{1-x} which provides highly active sites for water dissociation, with an activation energy of 0.56 eV[61], producing a greater number of surface hydroxyl groups and thus accelerating the ammonia oxidation reaction at the interface between the small well-dispersed Pt nanoparticles and MoC_{1-x}. This has been proven by Baek *et al.* who recently showed that MoC_{1-x} as a support and promoter enhances water dissociation capability in alkaline media [62] which made Pt/ MoC_{1-x} superior in hydrogen evolution to Pt/C. The decrease in the half and peak potentials of Pt/DG-MoC as compared to Pt/C implies the close proximity of the DG-MoC substrate and Pt nanoparticles that favours a strong synergistic effect between the nanoparticles by generating new bifunctional active centers in addition to platinum surface. The close proximity between the Pt and the Molybdenum carbide particles also evidenced from the spectra in Figure 4B indicates a partial charge transfer from Pt to the molybdenum compound in comparison to non-platinized DG-MoC. The shift indicates a strong electron interaction between the Pt and Mo, as observed previously for Pt/Mo_2C and also Co- and Mn-containing catalysts and their supports [55-58,50]. The bifunctional catalyst, in which there are sites for dissociating O–H bonds (on MoC next to Pt) in proximity to N–H bonds (on Pt), has the potential to reduce the activation energy for the dissociation of ammonia. Therefore, a shift in the onset potential is expected and indeed confirmed by our experiments. Similar effect was also recently observed for the reforming of methanol on Pt/α-MoC catalysts[61].

The cyclic voltammograms recorded up to very high oxidation potential beyond the practical ammonia oxidation region for testing the resilience of the catalysts. The results show that the

metal-support interaction leads to a lower current drop in the second voltammogram at the peak position which is approximately 20.7% for Pt/C and 3.6% for Pt/DG-MoC and reveals that Pt/DG-MoC is more resistant to ammonia poisoning.

4. CONCLUSION

In summary, high-resolution microscopy and spectroscopy confirmed the formation of graphene-encapsulated molybdenum carbide nanoparticles ensemble in nano-spheres for DG-MoC, and well dispersed Pt nanoparticles on DG-MoC for the Pt/DG-MoC catalysts. Nano-structured molybdenum carbide on an N-doped carbon-based support (DG-MoC) was found for the first time to have significant synergistic effects on the catalytic activity of platinum nanoparticles toward ammonia oxidation in alkaline media. XPS investigations revealed a partial charge transfer between Mo and Pt. Electrochemical studies of DG-MoC and NG for ammonia electro-oxidation in alkaline solution did not demonstrate any catalytic activities, while Pt/DG-MoC over-performed the-state-of-the-art Pt/C system with a 28 mV decrease in its half potential, 14 mV at peak potential and 23% higher oxidation current. The enhancement in the current density of Pt/DG-MoC can be ascribed to the presence of numerous hydroxyl groups on MoC_{1-x} which, at the interface with Pt nanoparticles, facilitate the oxidation reaction. The observed improvement of the onset potential is explained using the experimentally measured shift in XPS binding energies of the Mo compounds, which indicates a charge transfer to the Mo compounds upon depositing platinum and therefore, a synergistic interaction between MoC_{1-x} and Pt for the oxidation of ammonia.

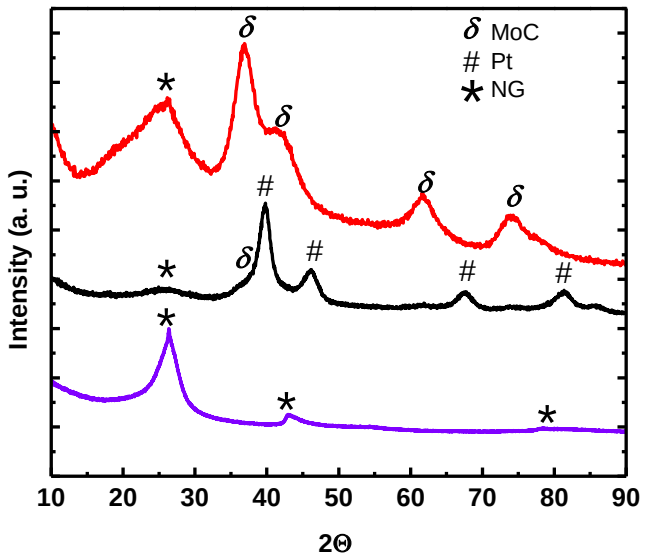

Figure 1. XRD patterns of the NG (blue), DG-MoC (red), and Pt/DG-MoC (black) catalysts.

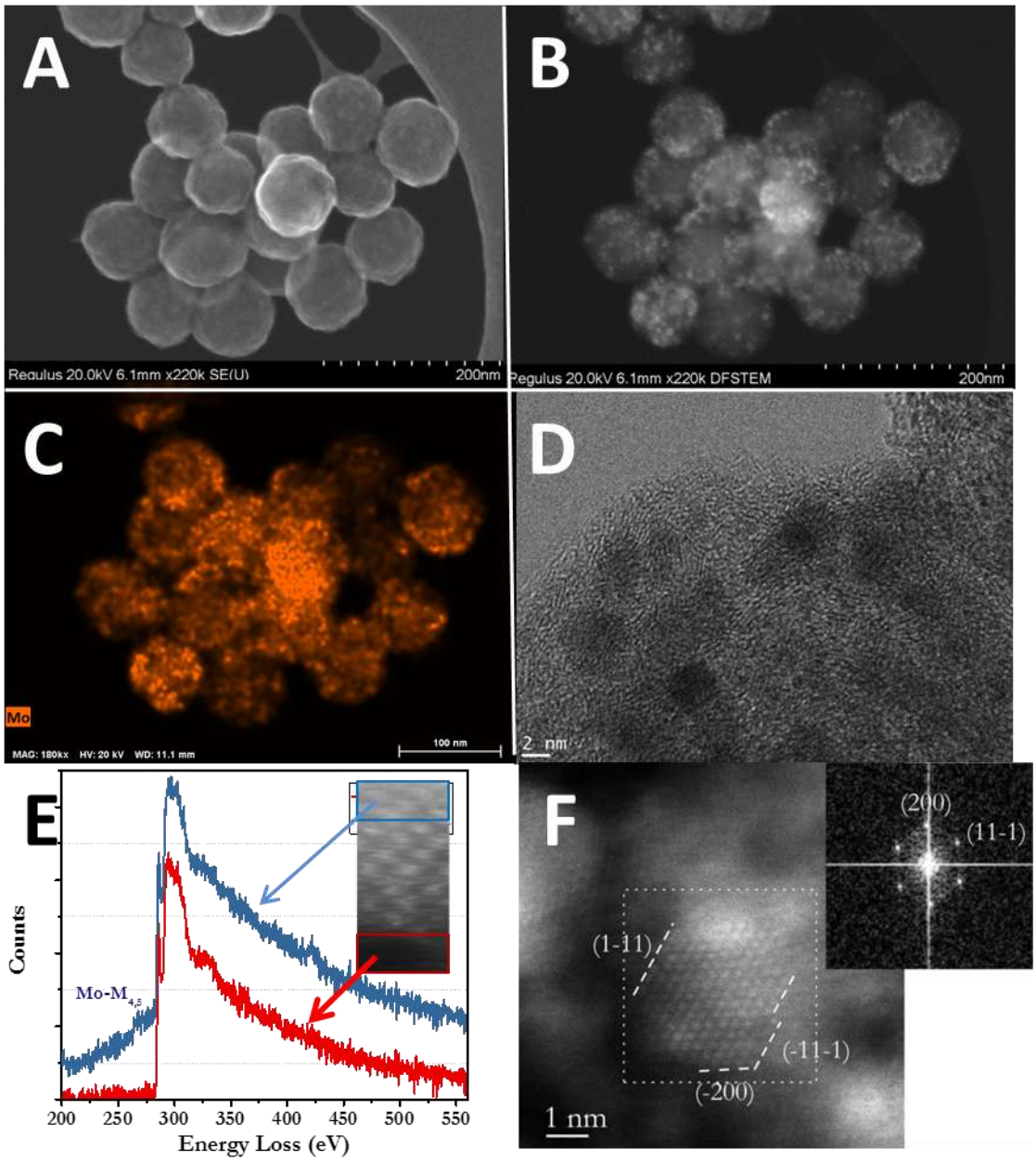

Figure 2. (A) Secondary electron (SE) SEM image of DG-MoC. (B) DF-STEM image and (C) EDX mapping for Mo- Lα. (D) High resolution BF-STEM image of MoC nanoparticles encapsulated by doped graphene layers. (E) EEL spectra averaged over 40x17 pixels (pixel size 0.027 nm) from areas indicated in the HAADF image recorded simultaneously (inset). Blue line corresponds to molybdenum carbide nanoparticles area and red line to the graphene shell (Dispersion is 0.3 eV/channel and exposure 0.02

seconds). (F) HAADF image of a molybdenum carbide nanoparticle and its corresponding FFT (inset).Facets along the planes {111} and {200} are indicated in the image.

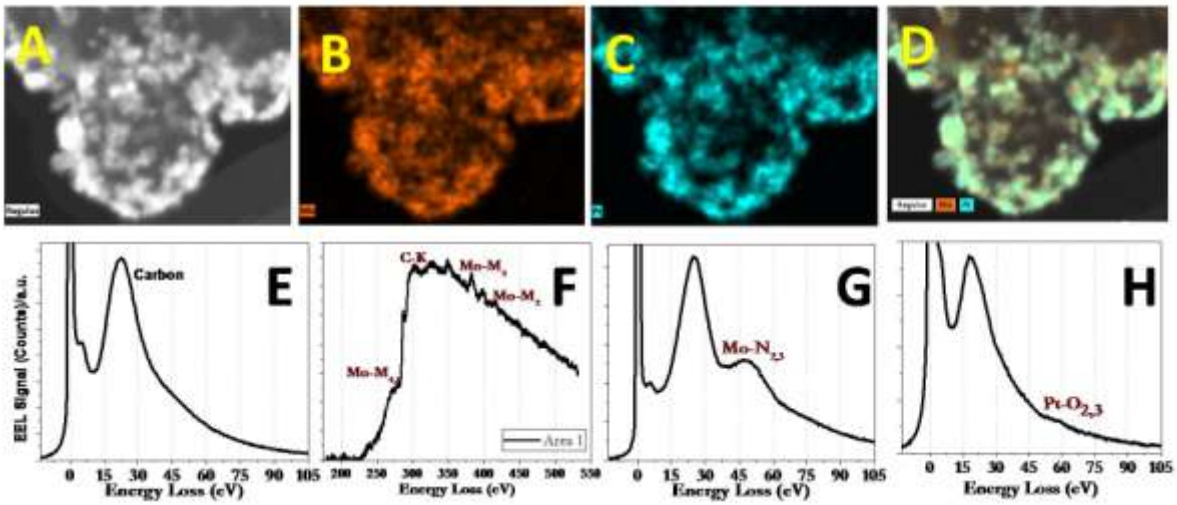

Figure 3. (A) Secondary electron (SE) SEM image of Pt/DG-MoC (scale bar=30 nm).(B) EDX mapping for Mo- Lα, (C) platinum and (D) Combined Pt and Mo signals superposed to the SE image shown in (A). EEL spectra recorded on doped carbon region with (E) no nanoparticles and with (F) MoC nanoparticles displaying the relevant edges on the core-loss region and (G) low-loss spectral region. (H) EEL spectrum of platinum nanoparticles shows a shoulder in low-loss energy area (Dispersion is 0.3 eV and exposure time 0.2 seconds). EEL spectra in (E), (G) and (H) were averaged over 4x13 pixels, while (F) is the average of EEL spectra over 37x17 pixels(Pixel size for all of them was 0.057 nm).

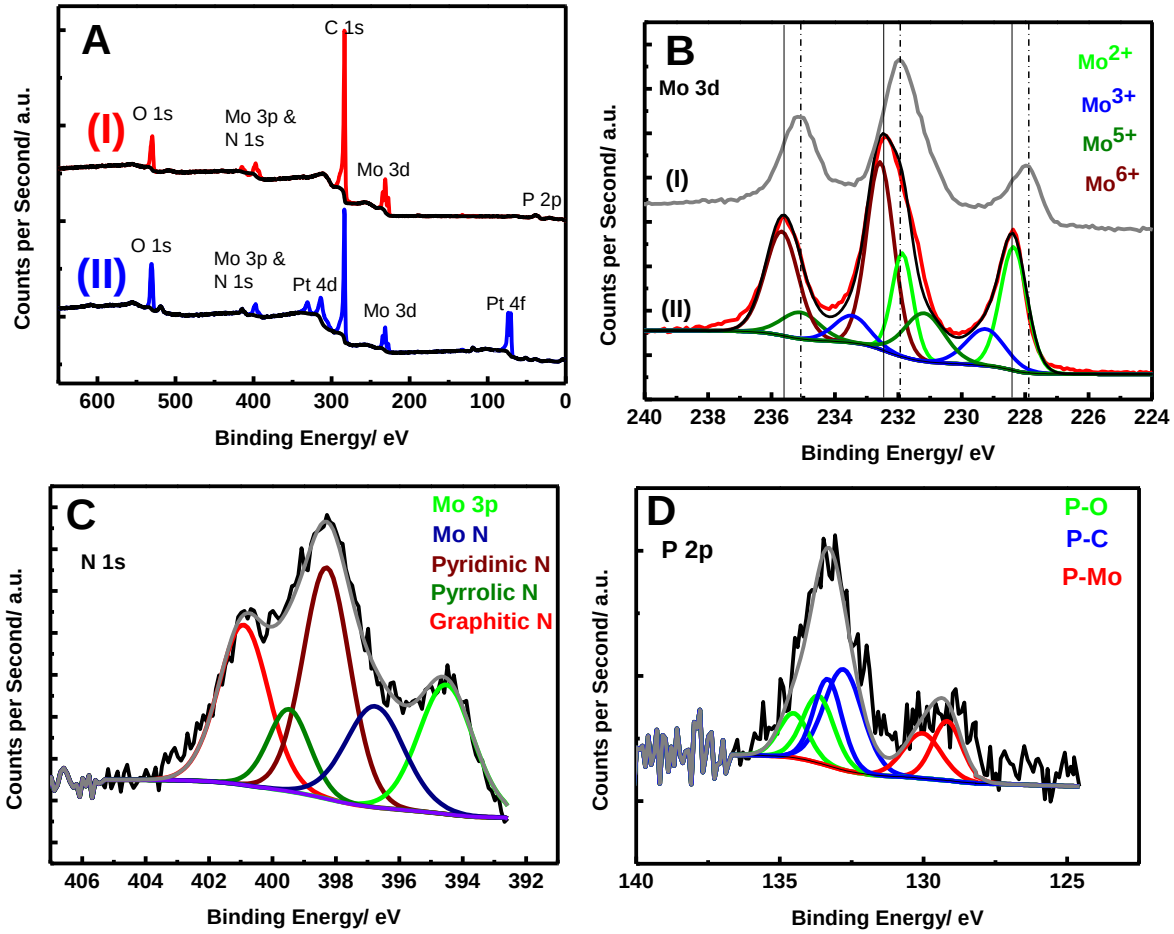

Figure 4.XPS survey spectra of DG-MoC (A-I) and Pt/DG-MoC (A-II) catalysts. B) XPS spectra of Mo 3d region of DG-MoC (II) and Pt/DG-MoC (I) catalysts. The inserted text colour matches the corresponding peak colour. Y axis presents different scales for each spectrum. C) Deconvoluted XPS spectrum of N 1s area of DG-MoC. D) XPS components of the deconvoluted P2p region of DG-MoC catalyst.

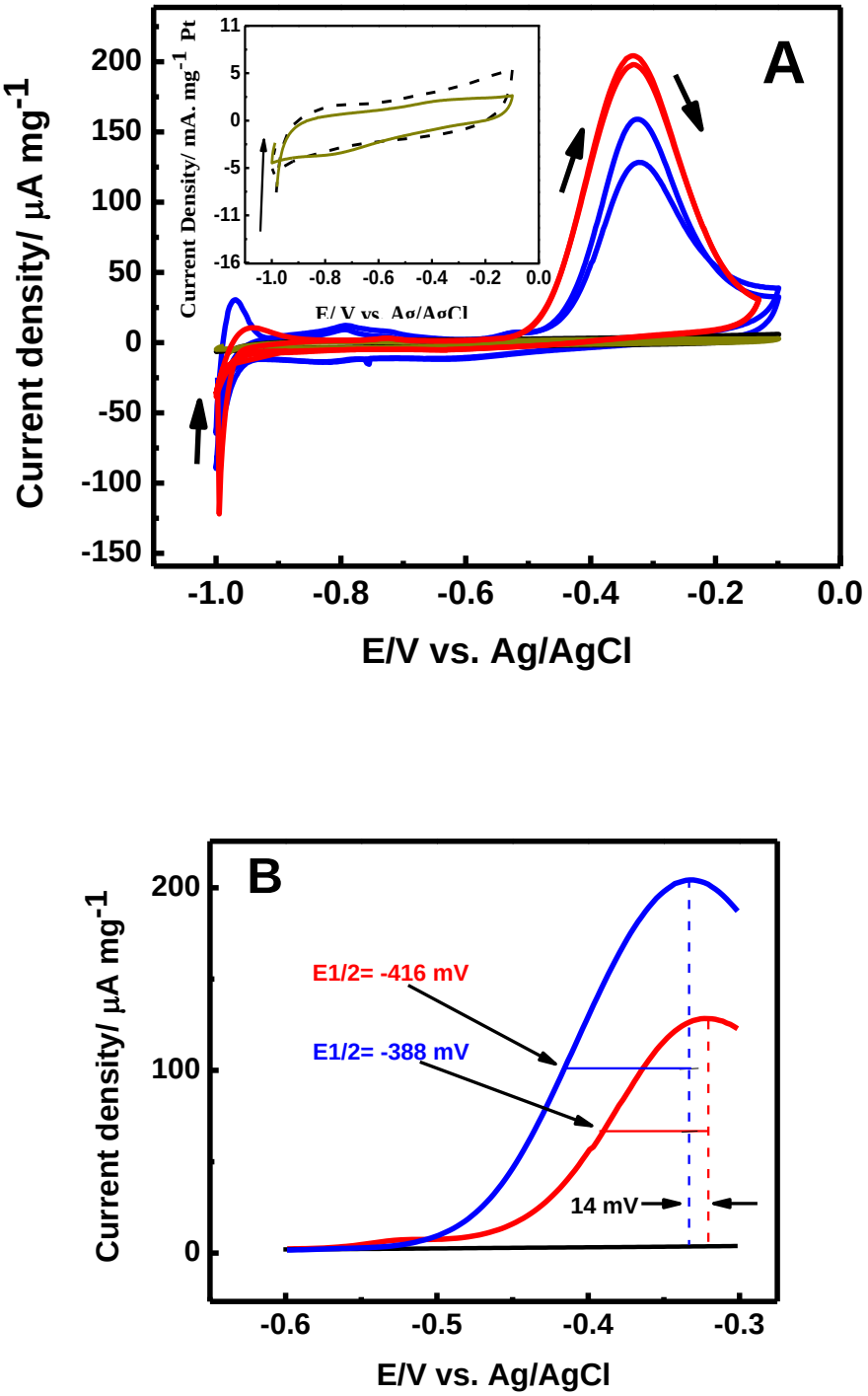

Figure 5. A) Cyclic voltammogarms of 10% Pt/C (red line), Pt/DG-MoC (blue line), NG (green line in main figure and the insert) and DG-MoC (black dashed line in main figure and the insert) in N_2 saturated

0.2 M NaOH + 0.1M NH_3 solution (loading is 0.3 mg cm^{-2}). B) Linear scanning voltammogarms of 10% Pt/C (red line) and Pt/DG-MoC (blue line) with their half peak potentials (E1/2) and peak potentials.

Acknowledgements

SuperSTEM is the UK National Research Facility for Advanced Electron Microscopy, supported by the Engineering and Physical Science Research Council (EPSRC). Dr. Jose Portoles for XPS experiments, Dr. Yukari Dan for assisting in SEM imaging and Mrs. Maggie White from Newcastle University for recording the X-ray diffractogram area acknowledged. Funding is acknowledged from Creating Knowledge Platform Challenges fund.

AUTHOR INFORMATION

Corresponding Author

m.bayati@shu.ac.uk

ASSOCIATED CONTENT

SUPPORTING INFORMATION

Supporting Information is available from the American Chemical Society Online Library or from the author.

CONFLICT OF INTEREST

The authors declare no conflict of interest.

REFERENCES

1. Rees, N. V.; Compton, R. G. Carbon-free energy: a review of ammonia- and hydrazine-based electrochemical fuel cells *Energy Environ. Sci.* **2011**, *4,* 1255–1260.
2. Sch¨uth, F.; Palkovits, R.; Schl¨ogl, R.; Su, D. S. Ammonia as a possible element in an energy infrastructure: catalysts for ammonia decomposition *Energy Environ. Sci.* **2012** *,* 5 ,6278–6289.
3. Cairns, E. J.; Simons, E. L.; Tevebaugh, A. D. Ammonia–oxygen fuel cell *Nature* **1968** , 217, 780–781.
4. Cheddie, D. Hydrogen Energy, Chapter 13 : Ammonia as a Hydrogen Source for Fuel Cells: A Review, **2012** Intech Open, Rijeka.
5. Vitse, F.; Cooper, M.; Botte, G. G. On the use of ammonia electrolysis for hydrogen production J. *Power Sources* **2005**, *142,*18–26.
6. B. K. Boggs, G. G. Botte, On-board hydrogen storage and production: An application of ammonia electrolysis *J. Power Sources,* **2009**, *192,*573–581.
7. Bonnin, E. P.; Biddinger, E. J.; Botte, G. G. Effect of catalyst on electrolysis of ammonia effluents *J. Power Sources* **2008**, *182,*284–290.
8. Vidal-Iglesias, F. J.; Solla-Gull´on, J.; Feliu, J. M.; Baltruschat, H.; Aldaz, A. DEMS study of ammonia oxidation on platinum basal planes *J. Electroanal. Chem.* **2006**, 588, 331–338.
9. L´opez de Mishima, B.A.; Lescano, D.; Molina Holgado, T.; Mishima, H. T. Electrochemical oxidation of ammonia in alkaline solutions: its application to an amperometric sensor *Electrochim. Acta,* **1998**, *43,* 395–404.

10. Vitse, F.; Cooper, M.; Botte, G.G. On the use of ammonia electrolysis for hydrogen production *J. Power Sources,* **2005**, *142,* 18 ,
11. Satyapal, S.; Petrovic, J.; Read, C.; Thomas G.; Ordaz, G. Progress towards Meeting Hydrogen-Powered Vehicle Requirements *Catal. Today,* **2007**, *120,* 246–256.
12. Liu, Y.; Yu, G.; Li, G.-D.; Sun, Y.; Asefa, T.; Chen, W.; Zou, X. Coupling Mo_2C with Nitrogen-Rich Nanocarbon Leads to Efficient Hydrogen-Evolution Electrocatalytic Sites. *Angew. Chem., Int. Ed.* **2015**, *54,* 10752−10757.
13. Porosoff, M. D.; Yang, X. F.; Boscoboinik, J. A.; Chen, J. G. G. Molybdenum Carbide as Alternative Catalysts to Precious Metals for Highly Selective Reduction of CO_2 to CO. *Angew. Chem., Int. Ed.* **2014**, *53,* 6705−6709.
14. Hyeon, T. H.; Fang, M. M.; Suslick, K. S. Nanostructured molybdenum carbide: Sonochemical synthesis and catalytic properties. *J. Am. Chem. Soc.* **1996**, *118,* 5492−5493.
15. Esposito, D. V.; Hunt, S. T.; Kimmel, Y. C.; Chen, J. G. G. A New Class of Electrocatalysts for Hydrogen Production from Water Electrolysis: Metal Monolayers Supported on Low-Cost Transition Metal Carbides. *J. Am. Chem. Soc.* **2012**, *134,* 3025−3033.
16. Hunt, S. T.; Nimmanwudipong, T.; Roman-Leshkov, Y. Engineering Non-sintered, Metal-Terminated Tungsten Carbide Nanoparticles for Catalysis. *Angew. Chem., Int. Ed.53* (**2014**) 5131−5136.
17. Patterson, P. M.; Das, T. K.; Davis, B. H. Carbon monoxide hydrogenation over molybdenum and tungsten carbides *Appl. Catal. A* **2003** *, 251,* 449-455.

18. Liu, W.; Chen, B.; Duan, X. ; Wu, K.-H. ; Qi , W.; Guo, X.; Zhang , B.; Su, D. Molybdenum Carbide Modified Nanocarbon Catalysts for Alkane Dehydrogenation Reactions *ACS Catal.,* **2017**, *7* ,5820–5827.
19. Claridge, J. B.; York, A. P.E.; Brungs, A. J.; Marquez-Alvarez, C.; Sloan, J.; Tsang, S. C.; Green, M. L.H. New Catalysts for the Conversion of Methane to Synthesis Gas: Molybdenum and Tungsten Carbide *J. Catal.* **1998**, *180,* 85-100.
20. Li, J.-S.; Wang, Y.; Liu, C.-H.; Li, S.-L.; Wang, Y.-G.; Dong, L.-Z.; Dai, Z.-H.; Li, Y.-F.; Lan, Y.-Q. Coupled molybdenum carbide and reduced graphene oxide electrocatalysts for efficient hydrogen evolution *Nature Commun.* **2016**, *7,* 11204.
21. Tang, Y.-J.; Gao, M.-R.; Liu, C.-H.; Li, S.-L.; Jiang, H.-L.; Lan, Y.-Q.; Han, M.; Yu, S.-H. Porous Molybdenum-Based Hybrid Catalysts for Highly Efficient Hydrogen Evolution *Angew. Chem. Int. Ed.* **2015** , *54,*12928 –12932.
22. Wan, C.; Regmi, Y. N.; Leonard, B. M. Multiple Phases of Molybdenum Carbide as Electrocatalysts for the Hydrogen EvolutionReaction. *Angew. Chem., Int. Ed.* **2014**, *53,* 6407−6410.
23. Zheng, W.; Cotter, T.P.; Kaghazchi, P.; Jacob, T.; Frank, B.; Schlichte, K.; Zhang, W.; Su, D.S.; Schüth, F.; Schlögl, R. Experimental and theoretical investigation of molybdenum carbide and nitride as catalysts for ammonia decomposition *J Am Chem Soc.* 2**013**, *135,* 3458-64
24. Siddharth, K.; Chan, Y.; Wang, L.; Shao, M. Ammonia electro-oxidation reaction: Recent development in mechanistic understanding and electrocatalyst design Current Opinion in *Electrochemistry* **2018**, *9,* 151-157.

25. Kojima, k.; Aika, K. I. Molybdenum nitride and carbide catalysts for ammonia synthesis *Appl. Catal., A*. **2001**, *219,*141-147.

26. Jacobsen, C. J. H.; Dahl, S.; Clausen, B. S.; Bahn, S.; Logadottir, A.; Norskov, J. K. Catalyst Design by Interpolation in the Periodic Table: Bimetallic Ammonia Synthesis Catalysts *J. Am. Chem. Soc.* **2001**, *123,* 8404 – 8405.

27. Schlögl, R. Handbook of Heterogeneous Catalysis; Ertl, G.; Knözinger, H.; Schüth, F.; Weitkamp, J. Eds.; Wiley-VCH: Weinheim, Germany, **2008**; Vol. 12.

28. R. Schlögl, Catalytic Synthesis of Ammonia—A "Never-Ending Story"? *Angew. Chem., Int. Ed.* **2003**, *42,*2004−2008.

29. Logadottir, A.; Rod, T. H.; Nørskov, J. K.; Hammer, B.; Dahl, S.; Jacobsen, C. J. H.; The Brønsted–Evans–Polanyi Relation and the Volcano Plot for Ammonia Synthesis over Transition Metal Catalysts *J. Catal.* **2001** ,*197,* 229−231. B)

30. Matanovic, I.; Garzon, F. H.; Nitrogen electroreduction and hydrogen evolution on cubic molybdenum carbide: a density functional study *Phys. Chem. Chem. Phys.* **2018** *, 20,* 14679-14687.

31. Yan, Z.; Xiea, J.; Shen, P. K. Hollow molybdenum carbide sphere promoted Ptelectrocatalyst for oxygen reduction and methanol oxidation reaction *J. Power Sources* **2015**, *286,* 239-246.

32. Elbaz, L.; Kreller, C. R.; Henson, N. J.; Brosha, E. L. Electrocatalysis of oxygen reduction with platinum supported on molybdenum carbide-carbon composite. *J. Electroanal. Chem.* **2014**, *720,* 34−40.

33. Yan, Z. X.; Zhang, M. M.; Xie, J. M.; Shen, P. K. An ultrastablebimetallic carbide as platinum electrocatalyst support for highly activeoxygen reduction reaction. *J. Power Sources* **2015** ,*295,* 156−161.

34. Schweitzer, N. M.; Schaidle, J. A.; Ezekoye, O. K.; Pan, X.; Linic, S.; Thompson, L. T. High Activity Carbide Supported Catalysts for Water Gas Shift *J. Am. Chem. Soc.* **2011**, *133,* 2378–2381.

35. Zhao, Y.; Kamiya, K.; Hashimoto, K.; Nakanishi, S. In situ CO_2-emission assisted synthesis of molybdenum carbonitride nanomaterial as hydrogen evolution electrocatalyst. *J. Am. Chem. Soc.* **2015**, *137*,110–113.

36. Kamat, P. V. Graphene-based nanoarchitectures. anchoring semiconductor andmetal nanoparticles on a two-dimensional carbon support. *J. Phys. Chem. Lett.* **2009**, *18,*
    a. 520–527.

37. Li, H.; Pang, S.; Feng, X.; Mullen, K.; Bubeck, C. Polyoxometalate assisted photo-reduction of graphene oxide and itsnano-composite formation. *Chem. Commun.* **2010**, *46,* 6243−6245.

38. Chen, Y.-Y.; Zhang, Y.; Jiang, W.-J.; Zhang, X.; Dai, Z.; Wan, L.-J.; Hu, J.-S. Pomegranate-like N,P-doped Mo2C@C nanospheres as highly active electrocatalysts for alkaline hydrogen evolution *ACS Nano,* **2016** ,*10,* 8851–8860.

39. Zhou, D.; Cui, Y.; Xiao, P. W.; Jiang, M. Y.; Han, B. H.; A General and Scalable Synthesis Approach to Porous Graphene. *Nat. Commun.* **2014**, *5,* 4716.

40. Qiua, J.; Yanga, Z.; Lia, Q.; Lib, Y.; Wua, X.; Qia, C.; Qiao, Q. Formation of N-doped molybdenum carbide confined into hierarchical and hollow carbon nitride microspheres with enhanced sodium storage properties *J. Mater. Chem. A,* **2016**, *4,* 13296-13306.

41. A. Gilewicz, R. Jedrzejewski, A. E. Kochmanska, B. Warchlinski, Structure of MoCN films deposited by cathodic arc evaporation, *Thin Solid Films* **2015**, *577,* 94-96.
42. Nakajima, T.; Shirasaki, T. Chemical Vapour Deposition of Tungsten Carbide, Molybdenum Carbide Nitride and Molybdenum Nitride Films*, J. Electrochem. Soc.* **2007** ,*144,* 2096-2100.
43. Yang, M.; Cai, Q.; Liu, C.; Wu, R.; Sun, D.; Chen, Y.; Tanga, Y.; Lu, T. Mono-dispersed hollow platinum nanospheres: facile synthesis and their enhanced electrocatalysis for methanol oxidation *J. Mater. Chem. A* **2014** *, 2,* 13738-13743.
44. Zou, Y.; Kinloch, I. A.; Dryfe, R. A. W. Mesoporous Vertical Co_3O_4 Nanosheet Arrays on Nitrogen-Doped Graphene Foam with Enhanced Charge-Storage Performance *ACS Appl. Mater. Interfaces* **2015** ,*7,* 22831 –22838;
45. Li, Z. Q.; Lu, C. J.; Xia, Z. P.; Zhou, Y.; Luo, Z. X-ray diffraction patterns of graphite and turbostratic carbon *Carbon* **2007**, *45,* 1686 –1695.
46. Bayati, M.; Abad, J. M.; Nichols, R. J.; Schiffrin D. J. Substrate Structural Effects on the Synthesis and Electrochemical Properties of Platinum Nanoparticles on Highly Oriented Pyrolytic Graphite *J. Phys. Chem. C* **2010** ,*114,*18439–18448.
47. Schweitzer, N. M.; Schaidle, J. A.; Ezekoye, O. K.; Pan, X.; Linic, S.; Thompson, L. T. High Activity Carbide Supported Catalysts for Water Gas Shift *J. Am. Chem. Soc.* **2011,** *133,*2378–2381.
48. Khademi, A.; Azimirad, R.; Zavarian, A. A.; Moshfegh, A. Z. Growth and Field Emission Study of Molybdenum Oxide Nanostars *J. Phys. Chem. C113* **2009,** 19298–19304.

49. Bayati, M.; Scott, K. Synthesis and activity of a single active site n-doped electro-catalyst for oxygen reduction *Electrochim. Acta* **2016**, *213,* 927 –932.

50. Bayati, M.; Scott, K. Secondary Impact of Manganese on the Catalytic Properties of Nitrogen-Doped Graphene in the Hydrogen Evolution Reaction *ChemCatChem9* (2017) 1 – 5.

51. Cao, B.; Veith, G. M.; Neuefeind, J. C.; Adzic, R. R.; Khalifah, P. G. Mixed Close-Packed Cobalt Molybdenum Nitrides as Non-noble Metal Electrocatalysts for the Hydrogen Evolution Reaction *J. Am. Chem. Soc.* **2013**, *135,* 19186−19192.

52. Kibsgaard, J.; Jaramillo, T. F. Molybdenum Phospho-sulfide: An Active, Acid-Stable, Earth-Abundant Catalyst for the Hydrogen Evolution Reaction *Angew. Chem. Int. Ed.* **2014** *53,*1 – 6.

53. Yan, H.; Tian, C.; Wang, L.; Wu, A.; Meng, M.; Zhao, L.; Fu, H. Phosphorus-Modified Tungsten Nitride/Reduced Graphene Oxide as a High-Performance, Non-Noble-Metal Electrocatalyst for the Hydrogen Evolution Reaction. *Angew. Chem., Int. Ed.* **2015**, *54,* 6325−6329.

54. Puziya, A.M.; Poddubnayaa, O.I.; Sochab, R.P.; Gurgulb, J.; Wisniewskic, M. XPS and NMR studies of phosphoric acid activated carbons Carbon46 **2008**, *46*, 2113-2123.

55. Jiang, Z. J.; Jiang, Z.; Interaction Induced High Catalytic Activities of CoO Nanoparticles Grown on Nitrogen-Doped Hollow Graphene Microspheres for Oxygen Reduction and Evolution Reactions *Sci. Rep.* **2016**, *6*, 27081.

56. Xiao, Y.; Wang, X.; Wang, W.; Zhao, D.; Cao, M. Engineering hybrid between MnO and N-doped carbon to achieve exceptionally high capacity for lithium-ion battery anode *ACS Appl. Mater. Interfaces* **2014,** *6,* 2051 –2058.

57. Saha, S.; Martin, B.; Leonard, B.; Li, D. Probing synergetic effects between platinum nanoparticles deposited via atomic layer deposition and a molybdenum carbide nanotube support through surface characterization and device performance. *J. Mater. Chem. A*, **2016** *4*, 9253-9265.

58. Tan, S.; Wang, L.; Saha, S.; Fushimi, R. R.; Li, D. Active Site and Electronic Structure Elucidation of Pt Nanoparticles Supported on Phase-Pure Molybdenum Carbide Nanotubes *ACS Appl. Mater. Interfaces* **2017**,*11*, 9815-9822.

59. Liu, P.; Rodrigez, J. A.; Muckerman T. Desulfurization of SO_2 and Thiophene on Surfaces and Nanoparticles of Molybdenum Carbide: Unexpected Ligand and Steric Effects *J. Phys. Chem. B* **2004**, *108*, 15662-15670.

60. Katayama, Y.; Okanishi, T.; Muroyama, H.; Matsui, T.; Eguchi, K. Electrochemical Oxidation of Ammonia over Rare Earth Oxide Modified Platinum Catalysts *J. Phys. Chem. C* **2015**, 119, 9134−9141.

61. Lin, L.; Zhou, W.; Gao, R.; Yao, S.; Zhang, X.; Xu, W.; Zheng, S.; Jiang, Z.; Yu, Q.; Li, Y.-W.; Shi, C.; Wen, X. -D.; Ma, D. Low-temperature hydrogen production from water and methanol using Pt/α-MoC catalysts. *Nature* **2017**, *544* 80–83.

62. Baek, D. S.; Jung, G. Y.; Seo, B.; Kim, J. C.; Lee, H.-W.; Shin, T. J.; Jeong, H. Y.; Kwak, S. K.; Joo S. H. Ordered Mesoporous Metastable α-MoC_{1-x} with Enhanced Water Dissociation Capability for Boosting Alkaline Hydrogen Evolution Activity. *Adv. Func. Mater.* **2019,** *29*, 1901217.